NRIAG Journal of Astronomy and Geophysics 6 (2017) 336–348

Contents lists available at ScienceDirect

NRIAG Journal of Astronomy and Geophysics

journal homepage: www.elsevier.com/locate/nrjag

Full length article

Africa was still far south in the Late Ypresian: Paleomagnetic study on the early Eocene 'Minia' formation in central Egypt

H. Lotfy [a,*], M. Abu Heleika [a], R. Mostafa [b], D. Wahbah [c]

[a] Faculty of Science, Minia University, Minia 61519, Egypt
[b] National Research Institute for Astronomy and Geophysics [NRIAG], Egypt
[c] Faculty of Science, Assiut University, New Valley Branch, Kharga, Egypt

ARTICLE INFO

Article history:
Received 31 March 2017
Revised 4 October 2017
Accepted 13 October 2017
Available online 6 November 2017

ABSTRACT

The paleomagnetic study was carried out on three sections of the Late Ypresian "Minia" formation limestone, in order to shed light on the paleolatitude of northeast Africa upon the end of the Early Eocene. The initial study on the anisotropy of magnetic susceptibility [AMS] helped in confining the paleomagnetic sampling to the virtually isotropic limestone beds. The subsequent stepwise thermal demagnetization of the three-axis isothermal remanence acquired in one sample of each sampled site, revealed the limited contribution of goethite and hematite with the main remanence carrier magnetite in most samples.

The assessment of the natural remanence during the progressive stepwise thermal demagnetization [15–17 steps] of all samples, elucidated the early decay [<150 °C] of a present- day field [PDF] overprint component scattered around the magnetic field direction of the study area. Despite that, the anchored component in most samples was carried in magnetite, yet hematite was recorded in few sites. The visual inspection of the decay spectra in the orthogonal projections, followed by the determination of the best-fit line of every component using the principal component analysis [PCA] technique, differentiated between the magnetite- and hematite- remanence components:

1. The magnetite-anchored component, which was overwhelming in most samples, was antipodal with shallow to medium inclination, yielding a paleomagnetic North poles at 73.8°N/197.5°E. This component, which successfully passed the reversal test at 95% confidence level, was considered as the characteristic primary remanent direction of the "Minia" formation. This paleomagnetic pole was, consequently, considered as representing the African Plate in the Late Ypresian.
2. On the other hand, the hematite component had normal north-direction clustered around the present-day field [PDF] in the study area. The hematite paleomagnetic pole at 88.7°N/78.8°E, was considered as a PDF overprint acquired in few samples upon exposure to desert weathering and partial oxidation of their original magnetite to hematite.

The reasonable consistence of the obtained pole of the "Minia" formation with synchronous poles of the main tectonic units rotated to the African coordinates, point to its reliability. This pole revealed that upon the end of the Lower Eocene, Northeast Africa was still at a far south paleolatitude with respect to its present-day position. The location of Cairo which is now at latitude 30°N, was at 14.2°N paleolatitude during the late Ypresion. This means that Africa was about 16° of latitude south to its current latitude.

* Corresponding author.
E-mail address: hamza.loutfy@mu.edu.eg (H. Lotfy).

Peer review under responsibility of National Research Institute of Astronomy and Geophysics.

Production and hosting by Elsevier

1. Introduction

The early Paleogene was the time of a relative quiescence of the African Plate due to the slow rates of spreading in the South Atlantic domain between 65 and 49 Ma (Cande et al., 1988; Nürnberg and Müller, 1991). This relative stillness is reflected in the marginal basins within the South Atlantic domain by low rates of subsidence and in the Tethyan domain by the slow

https://doi.org/10.1016/j.nrjag.2017.10.002
2090-9977/

convergence between Africa and Europe (Dewey et al., 1989). Depositional unconformities are, frequently, recorded in southern Europe (Schawn, 1980) and in northern Africa as in Abu Gharadig basin (Bayoumi and Lotfy, 1987) and Sirte basin (Gumati and Kanes, 1985). Within the Indian Ocean domain, upon the end of the lower Eocene (ca. 49 Ma), the Indian plate tectonic translation was substantially decreased recording the time of its collision with the Eurasian plate (Patriat and Achache, 1984; Patriat and Segoufin, 1988).

Upon the advent of the middle Eocene, a conspicuous new plate reorganization was recorded associated with the abrupt change in the rotation pole of South America and Africa between 45 and 42 Ma (Cande et al., 1988; Nürnberg and Müller, 1991) leading to the end of the period of tranquility of the African Plate.

In Egypt, a strong tectonics was recorded in post Ypresian time, along the major transcontinental Guineo- Nubia lineament (Guiraud et al., 1985). In south Egypt [as Sinn el-Kaddab scarp and along Darb el-Arbaein south Kharga Oasis], the protrusion of the basement rocks through a thin sedimentary cover, as young as Ypresian age, and the substantial dipping of the overlying sedimentary rocks around (Issawi et al., 1999), obviously reflect post Ypresian tectonism. This tectonism initiated and/or re-activated many E-W faults in south Egypt. These faults are mostly normal with strike slip displacement (up to 700 ms). All these faults and up arching structures are intimate consequences of the transcontinental Guineo- Nubia lineament.

Concurrently, upon the close of the lower Eocene, a global gradual drop in the sea level started during the late Ypresian (Haq et al., 1988). Consequently, the Egyptian territory started a gradual emergence from south to north, resulting in a slow steady northward regression of the Tethys shore line reflected by the variation of the Eocene marine lithologies and their geographic northward off-lap. The first regression sedimentary rock unit of that time was named by Said (1960) as Minia formation which underlies the middle Eocene (Lutetian) milky white limestone of the Samalut formation and overlies the lower Eocene (Ypresian) flint limestone of the Thebes formation along the Nile Valley with apparent conformities (Said, 1990).

The present paleomagnetic study on the late lower Eocene Minia formation is, therefore, devoted to authenticate on the paleotectonic position of the African Plate upon the termination of its relative standstill time at the end of the Lower Eocene.

2. Geology and sampling

In central Egypt, at the latitude of Minia Governorate [28°N], the Eocene white limestone is exposed on both sides of the Nile Valley,

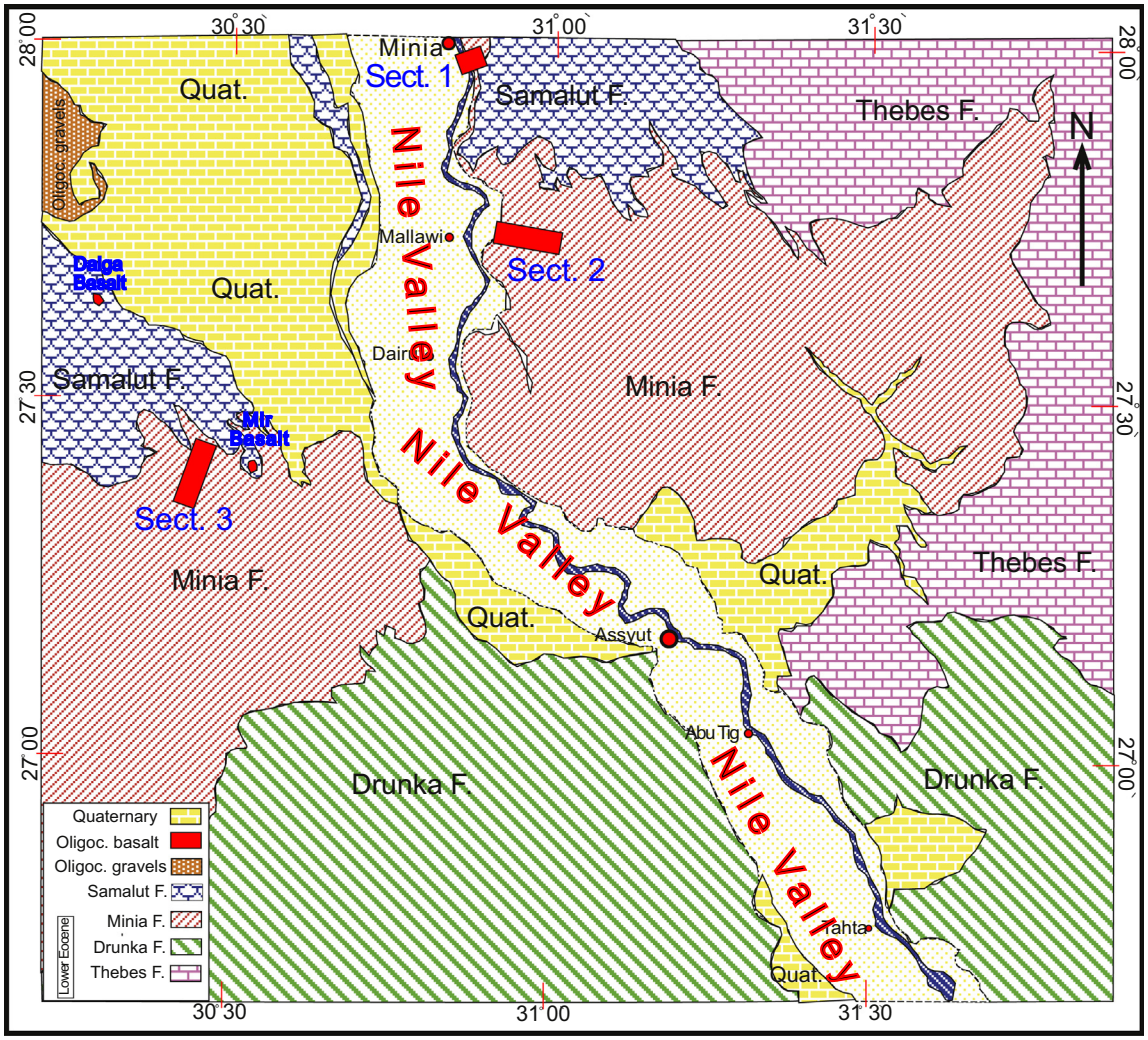

Fig. 1. Simplified geologic map after Klitzsch et al., (1987), showing the exposure of Minia formation and the location of the studied sections in the eastern and western deserts on both sides of the Nile Valley.

building prominent vertical scarps above the Nile Valley flood plain and developing persistent plateaus east and west of the valley. These scarps are made up of the Minia formation at the base and the Samalut formation at the top (Bishay, 1961).

At its type section, the Minia formation (Said, 1960, 1962; Bishay, 1961) designates +35 m of snow white Alveolinid limestone beds forming a characteristic vertical scarp with protruding hard limestone ledges east Minia city. This thickness, remarkably, increases further east and south along the deep valleys dissecting the limestone tablelands. The Minia formation was, originally, thought to be of early middle Eocene age (Said, 1960), until Boukhary et al., (1982a, 1982b) and Boukhary and Abdelmalik (1983) relegate its age to the late early Eocene (late Ypresian) based on its faunal assemblage. Philobbos and Keheila (1979) attributed the Minia formation to the deposition in bar and ramp coastal sub-environments.

In the present study, oriented samples were collected from three distant cliffy sections of the Minia formation plotted in a simplified geologic map after Klitzsch et al., (1987) (Fig. 1). Section I is located nearby to the type section east Minia city. Section II lies about 40 kms to the south of the first section, in the Eastern Desert to the east of Mallawi city. This section extended horizontally to about four kilometers along a deep valley extending NW-SE exposing fresh limestone samples. Section III is located about 80 kms southwest Minia city in the Western Desert. This section is a composite section collected from several subdued escarpments exposing fresh limestone.

Despite their fresh exposures, the cliffy nature of the limestone prevented the equal vertical spacing of the sampling sites. Moving laterally was the sole way to collected higher stratigraphic horizons in the same section. The sampled sections are entirely made of white limestone with few laterally-discontinuous softer yellowish marly limestone beds. Because of their monotonous nature of the lateral correlation between the sampled beds within the three different widely-spaced studied sections is unattainable.

Sampling was carried out in two separate field trips. In the first trip, oriented samples were collected vertically from various beds showing visual variations in color or hardness, to perform the preliminary anisotropy of magnetic susceptibility [AMS] study. The sampled beds were marked in the field, vertically, by serial numbers in each section using waterproof pens and their coordinates were recorded by the GPS. Only beds that show reasonable isotropy of their AMS were, subsequently, in the second field trip for the inspection of the paleomagnetic natural remanence. Sam-

Table 1
Measured and calculated anisotropy of magnetic susceptibility [AMS] parameters of beds in the studied sections. [km] mean susceptibility; [Pj] corrected anisotropy degree; [L] lineation; [F] foliation; [T] and [Q] factors for shape parameters for the susceptibility ellipsoid; [K1, K2, K3] are the declination and inclination of the three [Maximum, intermediate and minimum] magnetic susceptibility axes, respectively; * excluded beds.

Section No-bed No	$K_{m(*10\ SI\ unit)}^{-6}$	Pj	L	F	T	Q	Magnetic susceptibility axes [Dec°/Inc°]		
							K1	K2	K3
I-8	83.52	1.004	1.001	1.003	0.504	0.284	258/21	165/6	59/68
I-9	75.08	1.010	1.003	1.007	0.414	0.345	21/9	288/18	137/70
I-10	84.83	1.004	1.002	1.002	−0.028	0.693	285/69	165/11	72/18
I-11*	**25.01**	**1.002**	**1.004**	**1.000**	**−1.000**	**2.000**	**180/45**	**−0/45**	**90/0**
I-12	41.07	1.031	1.024	1.005	−0.651	1.412	137/15	33/43	241/43
I-14	194.55	1.006	1.001	1.005	0.607	0.218	148/33	318/57	55/4
I-15*	**14.93**	**1.108**	**1.016**	**1.083**	**0.661**	**0.193**	**104/30**	**201/13**	**311/57**
I-16	101.97	1.042	1.015	1.026	0.260	0.461	182/64	10/26	278/3
I-17	214.28	1.041	1.007	1.031	0.642	0.200	59/76	242/14	152/1
I-18	51.40	1.018	1.010	1.008	−0.111	0.773	32/24	257/58	131/20
I-19	55.23	1.020	1.015	1.004	−0.622	1.368	216/66	27/24	118/4
I-20	34.76	1.011	1.007	1.004	−0.267	0.930	235/2	327/47	143/43
I-21	26.19	1.010	1.005	1.005	0.047	0.627	0/90	22/0	112/0
I-22	57.40	1.007	1.003	1.004	0.106	0.577	144/12	260/52	45/35
I-23	46.09	1.007	1.001	1.006	0.634	0.202	180/54	90/0	−0/36
Range	26.19–214.3	1.004–1.042	1.001–1.024	1.002–1.031	(−0.651)–0.634	0.20–1.412			
Mean N = 13 beds	74.16	1.016	1.010	1.0126	0.118	0.6223	170.8//71.9	338.3/69.7	101.5/47.9
II-24	63.01	1.015	1.009	1.005	−0.249	0.912	140/81	37/2	306/9
II-25	51.39	1.009	1.005	1.004	−0.091	0.752	116/6	25/6	249/82
II-26*	**31.83**	**1.052**	**1.028**	**1.023**	**−0.097**	**0.768**	**318/10**	**197/71**	**51/16**
II-28*	**58.57**	**1.100**	**1.003**	**1.085**	**0.936**	**0.034**	**243/9**	**152/4**	**38/80**
II-29	108.64	1.029	1.014	1.014	−0.011	0.683	233/31	85/55	332/15
II-30	133.44	1.022	1.007	1.015	0.352	0.390	207/7	300/30	105/59
II-31	209.15	1.014	1.006	1.008	0.191	0.510	324/3	55/14	222/75
II-32	67.03	1.020	1.003	1.016	0.660	0.188	139/67	236/3	328/23
II-33	104.67	1.011	1.007	1.004	−0.283	0.947	166/22	54/42	275/40
II-34	94.87	1.008	1.004	1.004	−0.108	0.768	114/36	331/47	219/19
II-35	347.51	1.012	1.007	1.004	−0.316	0.983	6/48	225/35	120/20
II-36	247.05	1.004	1.001	1.003	0.272	0.446	59/55	272/30	173/16
Range	51.4–347.5	1.004–1.029	1.001–1.014	1.003–1.016	(−0.316)–0.660	0.188–0.983			
Mean N = 10 beds	145.86	1.014	1.0063	1.0077	0.042	0.654	141.3/53.0	352.2/57.5	262.7/69.1
III-46	189.11	1.008	1.003	1.005	0.253	0.460	328/46	227/11	127/42
III-47	37.40	1.061	1.007	1.048	0.756	0.133	135/0	45/0	0/90
III-48*	**18.33**	**1.103**	**1.049**	**1.051**	**0.017**	**0.674**	**81/67**	**316/14**	**221/18**
III-49	37.80	1.086	1.041	1.043	0.028	0.660	68/63	186/14	282/23
III-50*	**18.63**	**1.079**	**1.055**	**1.020**	**−0.465**	**1.174**	**107/7**	**327/81**	**197/6**
III-51	50.83	1.060	1.020	1.038	0.306	0.429	149/70	29/10	296/17
III-52	33.57	1.070	1.019	1.048	0.437	0.337	72/5	174/67	339/23
Range	33.6–189.1	1.008–1.086	1.003–1.041	1.005–1.048	0.028–0.756	0.133–0.660			
Mean N = 5 beds	69.74	1.057	1.018	1.0364	0.36	0.4038	88/54.4	138.2/68.2	304.4/56.5

pling for the paleomagnetic study was restricted to the beds free from of any distortion of their isotropy of their AMS and each of these beds was considered as a discrete sampling site.

3. Analysis of the anisotropy of magnetic susceptibility [AMS] parameters

The inspection of the anisotropy of magnetic susceptibility (AMS) was, initially, applied to verify the magnetic fabrics of the limestone beds constituting the three selected sections of the Minia formation in the study area prior to the paleomagnetic study.

Limestone samples are collected vertically from various beds constituting the total thickness of the exposed rocks in the study sections (Fig. 1). The samples were measured in the Paleomagnetic Laboratory of the National Research Institute of Astronomy and Geophysics [NRIAG] in Cairo, Egypt, following the standard procedures described in Jelinek (1978). The samples were subjected to the standard AMS measurements in different directions using the Kappa Bridge susceptibility meter MFK1-FA (by Agico- Brno). Since the beds are undisturbed, no tilt correction is made.

The selective AMS parameters; the mean magnetic volume susceptibility [km] (Nagata 1961), the magnetic foliation (F) (Stacey et al., 1960), the magnetic lineation [L] (Balsley and Buddington, 1960), the shape factor [T] (Jelinek, 1981), the Q- factor (Granar, 1958; Jelinek, 1981; Ellwood and Crick, 1988; Tarling and Hrouda, 1993) and the corrected anisotropy degree (Pj) (Jelinek, 1981) are calculated for each bed (Table 1). Six beds from the three sections were excluded due to their anomalous AMS parameters, before calculating the ranges and means of these parameters throughout the vertical thickness of each section and the overall ranges and means for each parameter within the Minia formation limestone in the study area.

The results of km, Pj, F, L, T and Q values show distinct variations for the different stratigraphic units (Table 1). The highest mean value of magnetic susceptibility (km) is observed in section II limestone, while the lowest is in section III. The overall calculated mean susceptibility [km] for the three sections of Minia formation limestone is ranging from 347.5×10^{-6} to 26.19×10^{-6} SI units with the mean value of 89.03×10^{-6} SI units suggesting the dominance of paramagnetic effects.

The magnetic lineation L and foliation F are rather weak in the study sections (Table 1). The overall maximum, minimum and mean values for the magnetic Lineation [L] of Minia formation limestone are 1.041, 1.001 and 1.010. The Foliation [F] ranges between 1.048 and 1.002 with a mean value of 1.015. The anisotropy degree (Pj) varies from 1.086 to 1.004 with average value of 1.0228. The ranges of the two shape factors [T] and [Q] are 0.756- (−0.691) and 1.412–1.133, respectively. Their means are 0.131 and 1.596, respectively.

The mutual graphical relations between various AMS parameters; the mean susceptibility [km] versus the corrected anisotropy degree [Pj], the Flinn diagram showing the relation between foliation [F] versus lineation [L] and the relation between T-factor versus the corrected degree of anisotropy, are plotted in (Fig. 2A–C) for inspecting of the possible eccentricity and the shape of susceptibility ellipsoid. The six excluded stratigraphic units due to their abnormal AMS parameters are highlighted by squares to reveal their ultimate position in the graphical plots (Fig. 2A–C). It is worth mentioning that the relation between the anisotropy degree Pj and the mean magnetic susceptibility K_m (Fig. 2A) reveals no definitive mutual relation.

The results of AMS measurements are, also, represented by second-rank tensor, which can be depicted as an ellipsoid with three mutually perpendicular principle axes, K1 ≥ K2 ≥ K3 representing the maximum, intermediate and minimum susceptibility axes, respectively (Rochette et al., 1992). The directions of the three principal magnetic susceptibility axes K1, K2 and K3, of various stratigraphic units forming the Minia formation in the study area, are plotted in equal area stereographic projection (Fig. 2D–F) in three different colors. The directions of the

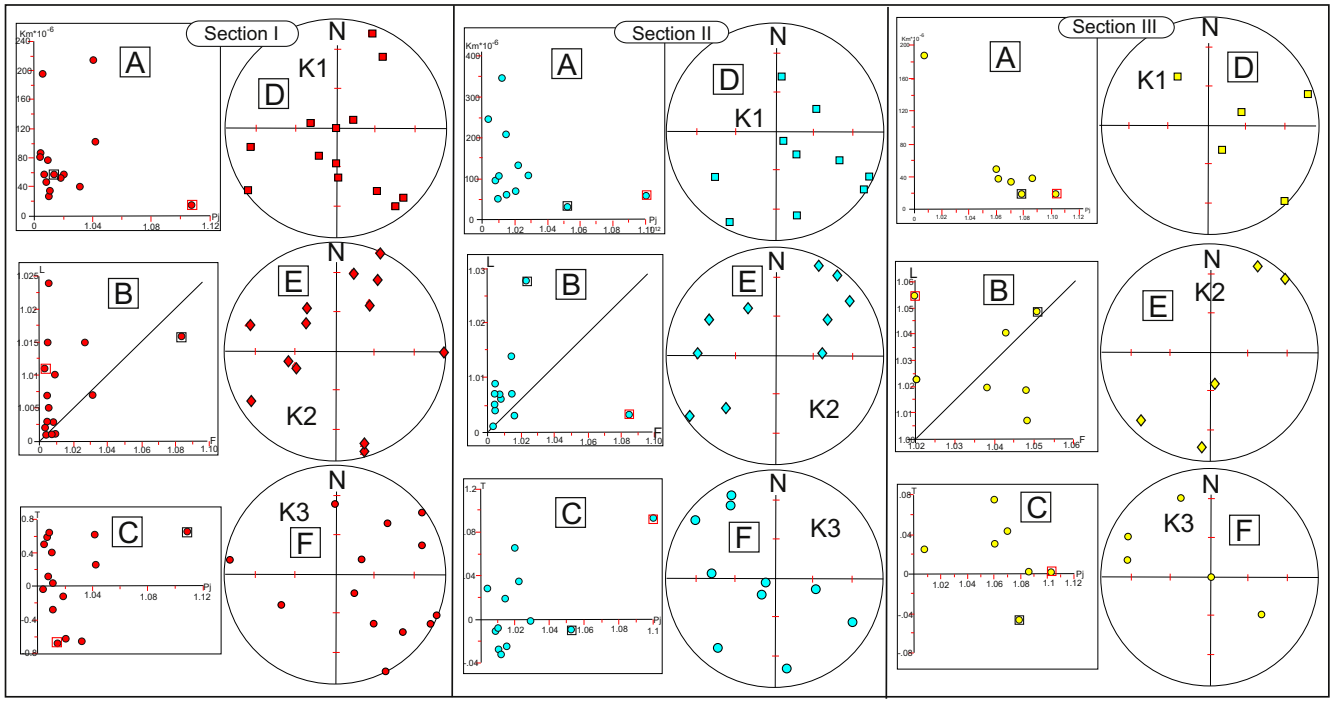

Fig. 2. A, B, C Graphical presentations and relationships between the measured and calculated anisotropy of the magnetic susceptibility [AMS] parameters in the three sections of Minia formation limestone in the study area presented in Table 1. D–F are the lower hemisphere equal-area projections of the anisotropy of magnetic susceptibility [AMS] data, D) K_1 axes (magnetic lineation), E) K_2 axes, and F) K_3 axes (magnetic foliation). Samples surrounded by squares are excluded from the calculated means, the stereographic projections and from the paleomagnetic study.

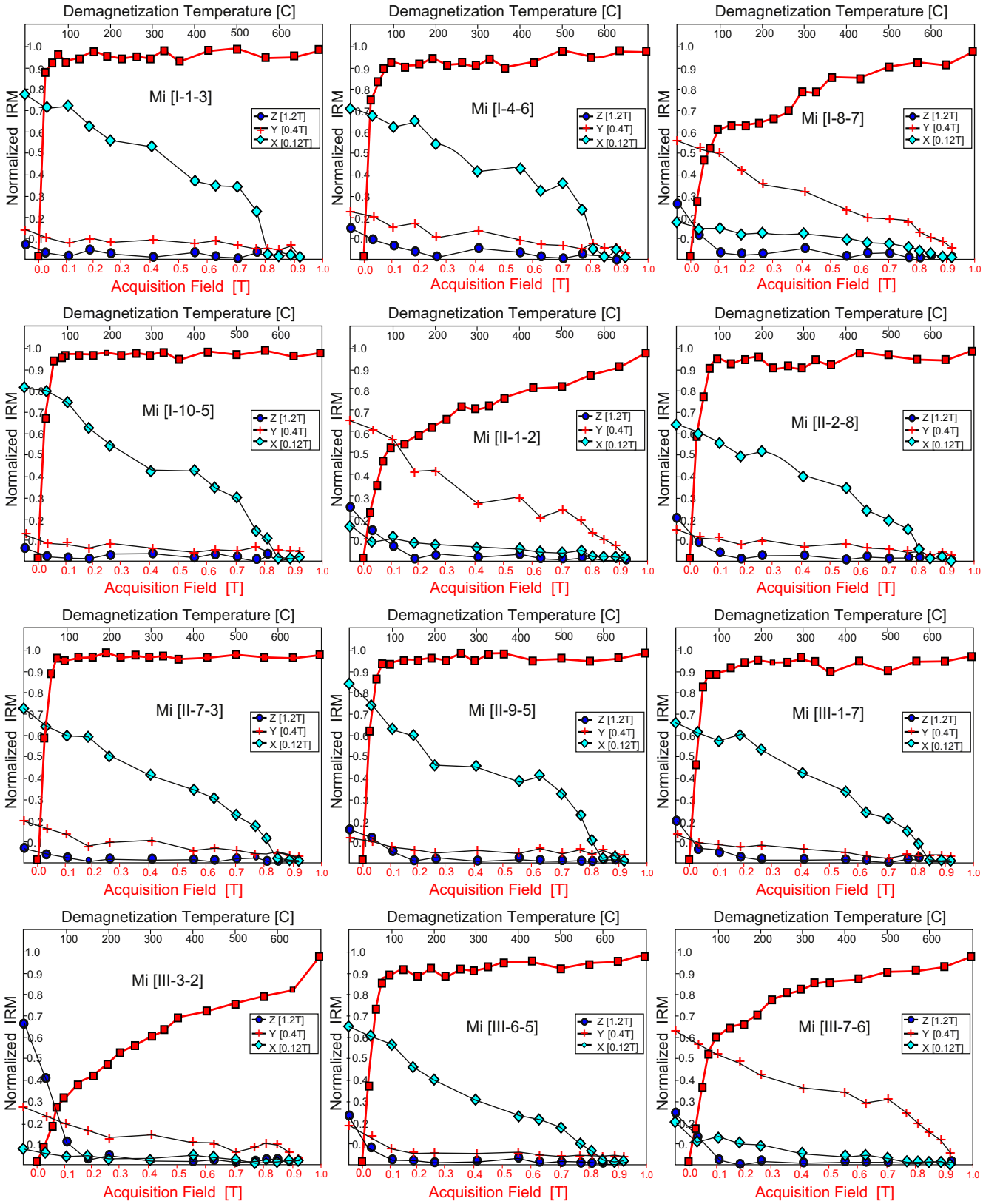

Fig. 3. The isothermal remanent demagnetization [IRM] study. The lower scale represents the acquired magnetic field during the progressive stepwise acquisition up to 1 Tesla (Heller, 1978). The upper scale shows the temperature during the progressive thermal demagnetization of the variable intensity IRM imparted along three orthogonal axes (Lowrie, 1990).

maximum axis K_1 (magnetic lineation), the intermediate axis K_2 and the minimum axis K_3 (magnetic foliation) are, generally, scattered in the stereographic projection. Their inclinations vary from very shallow to steep and their trends are widely distributed all over the stereographic projections (Fig. 2D–F)), with no preferred orientation.

Based on the inspection of the anisotropy of magnetic susceptibility [AMS] parameters of the selected stratigraphic units (Table 1), their graphical mutual relations and the directions of their main axes, it could be stated that the variability of the anisotropy magnetic susceptibility reflects differences in the content and type of the magnetic minerals responsible for the AMS components. The low anisotropy degree Pj (average 0.0228 SI units) indicates the virtual isotropism of the magnetic susceptibility. The magnetic fabric patterns, exemplified by the weak magnitudes of the AMS parameters (Table 1, Fig. 2A–C) and the scattered distribution in the directions of the three susceptibility axes (Fig. 2D–F), all indicate that the Minia formation limestones are implicitly isotropic and still hold their depositional primary fabric and might be free from any possible inclination shallowing errors which could in inherit or distort their primary natural remanence direction.

4. Isothermal remanent magnetization [IRM] study

The remanence carriers of the magnetic minerals in the collected samples were inspected through the study of their behavior during the progressive acquisition of the IRM up to one Tesla. Also, the observation of the thermal decay of three different intensities of IRMs [120 milliTesla along the X-axis, 400 mTesla along the Y-axis and 1200 mTesla along the Z-axis] (Fig. 3), acquired along three perpendicular axes in the samples during the stepwise thermal demagnetization (Lowrie, 1990), was applied to differentiate between the studied sites according to their magnetic minerals and the relative abundance of magnetite, hematite and goethite.

Initially, an IRN was progressively imparted in one representative sample/site using the following increments 25, 50, 75, 100, 150, 200, 250, 300, 350, 400, 450, 500, 600, 700, 800, 900 and 1000 mTesla. The inspection of the measured IRMs revealed two different behaviors (Fig. 3). Most sites showed an early sharp increase of the IRM in the first two or three increments. The majority of these samples reached stability and become saturated at 100 mT, then remained fluctuating without increase in their acquired IRM up to 1000 mTesla (Fig. 3). These samples reflect the predominance of magnetite. On the other hand, few samples like Mi [I.8.7], Mi [II.1.2], Mi [III.3.2] and Mi [III.7.6] (Fig. 3), started by an early increase in the acquired remanence, followed by continuous steady increase up to 1000 mTesla without reaching saturation. The sites represented by these samples are, apparently, dominated by hematite and/or goethite with minor contribution of magnetite.

In the subsequent step, three variable intensities of IRMs were induced along three perpendicular axes in one sample/site (Lowrie, 1990) then, thermally demagnetized stepwise (Fig. 3). Initially, 50 °C increments were applied until 200 °C, to unveil the IRM of the goethite. The 50 °C increment was maintained once again between 400 °C and 600 °C followed by 25 °C increments until complete demagnetization of the samples or 650 °C. The increments were capable to unveil the IRM decay of the magnetite and the hematite. The progressive thermal demagnetization of the three-axis IRM (Fig. 3) supported the domination of magnetite as the major remanence carrier in most samples. It, also, aided in the differentiation between hematite-dominated sites like Mi [I.8.7], Mi [II.1.2] and Mi [III.7.6] and those which are characterized by goethite as main remanence carrier as Mi [III.3.2] (Fig. 3).

The IRM study elucidated that the majority of the collected samples in three sections of the Minia formation limestone are dominated by magnetite with limited contribution of goethite and/or hematite. Goethite seems to be present in all samples with minor contribution. Samples, in which either magnetite or hematite is the main remanence carrier, proceeded to the thermal demagnetization study of the natural remanence, in order to inspect the natural remanence direction characterizing the magnetite- and the hematite- dominated sites. The goethite-dominated sites were discarded from the thermal demagnetization study of their natural remanence, as the goethite is a secondary alteration mineral, expected to reflect secondary magnetization

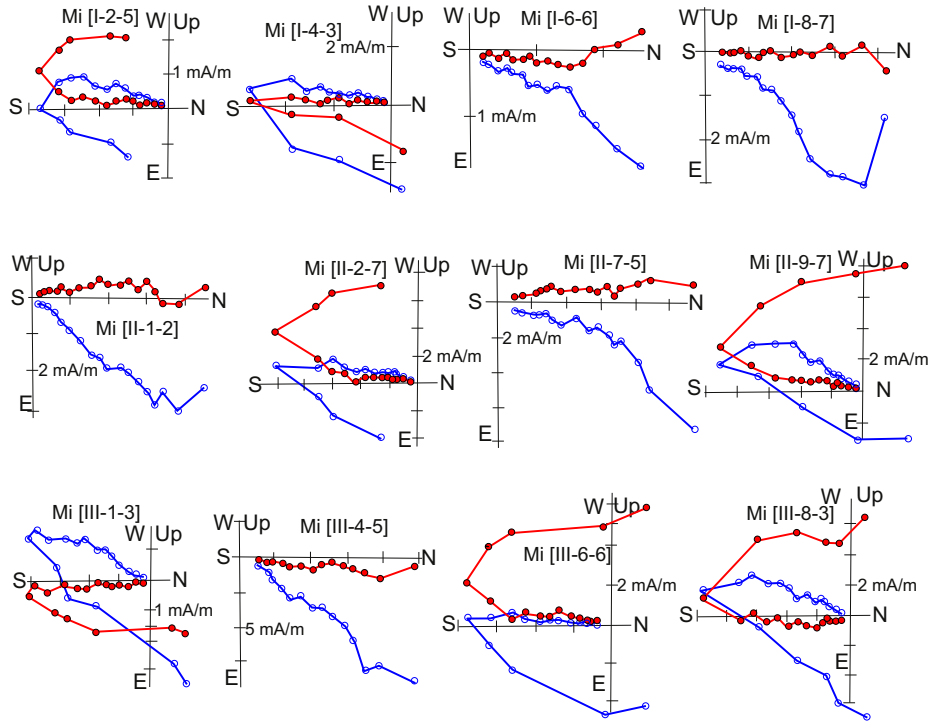

Fig. 4. Representative orthogonal projections of the thermally demagnetized samples (Zijderveld, 1967), showing the thermal decay and orientation changes of the natural remanence trajectories during the progressive thermal demagnetization of the Minia formation limestome. Open/filled circles in the diagrams correspond to vertical/horizontal projections.

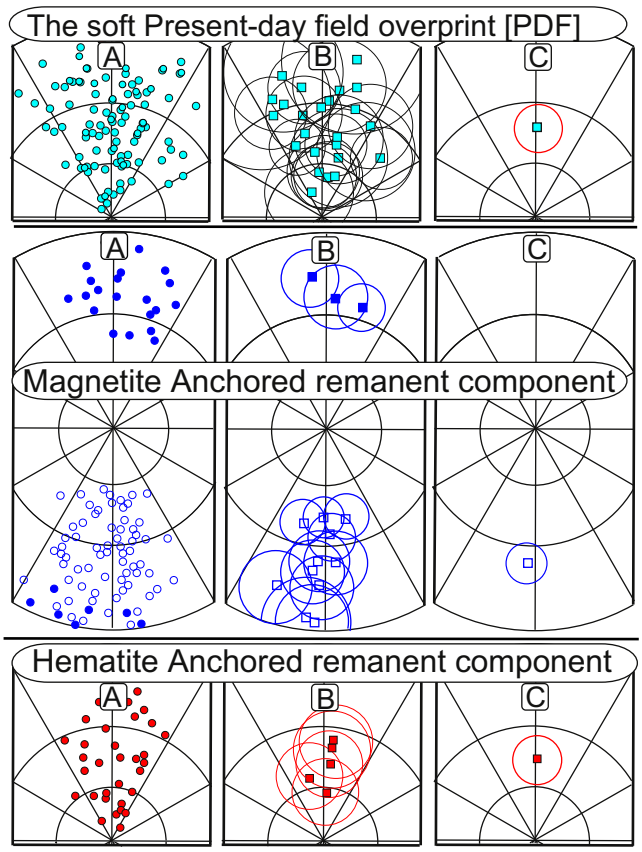

Fig. 5. Equal-area projections of the differentiated magnetic components of the natural remanence during progressive thermal demagnetization, [A] the individual sample directions, [B] the site-means directions with their associated semi-angles of the cones of 95% confidence [α95], [C] overall means of each isolated component with their overall α95s. The upper part represents the goethite-hosted component, the middle part shows the directions of the magnetite anchored component and the lower part manifests the hematite anchored component. Open/filled circles indicate upper/lower hemisphere projections. Data are listed in Table 2.

acquired in samples upon their weathering. Section III seems to contain more hematite/goethite samples.

5. Thermal demagnetization of the natural remanence

Samples of the magnetite- and hematite-dominated sites were exposed to progressive thermal demagnetization [13–17 steps]. In order to differentiate between the low-blocking and high-blocking temperature components in each sample, 50 °C increment was used from room temperature up to 200 °C and between 400 °C and 550 °C, then, smaller steps of 25 °C were applied above 550 °C until complete demagnetization.

The visual inspection of the demagnetization in the orthogonal projections (Zijderveld, 1967) of each sample, revealed that natural remanence of most samples displayed bi-vectorial decay. The thermal decay rates and the directional path changes of the natural remanence during progressive demagnetization were characterized by an early disintegration of a soft component at ≤150 °C. This component, which seems to be hosted in goethite, has north- oriented medium positive inclination (Fig. 4), almost parallel to the present-day magnetic field in the study area. This component represents a secondary present-day field [PDF] overprint.

In the magnetite-dominated samples, which represent the majority of the demagnetized sites, the decay path is characteristically bi-vectorial. The destruction of the PDF overprint is succeeded by the decay of a distinct shallower bi-polar antipodal anchored component decaying between 400 °C and 585 °C as their natural remanence vanishes. This magnetite component which has either a north-oriented down or a south-oriented up shallow inclination was significantly shallower than the PDF overprint in the demagnetized samples (Figs. 4 and 5 A [middle part]).

However, in few hematite-dominated sites, the decay path is steadily uni-vectorial. Upon the decay of the PDF overprint, the demagnetization trajectories do not change their direction. They retain their north-oriented medium inclination normal polarity parallel to the PDF, until complete demagnetization at temperatures >600 °C. Samples Mi [I.8.7], Mi [II.1.2] and Mi [III.4.5] (Fig. 4) are examples of this behavior. This behavior implies that

Table 2
The site means of magnetic components isolated after the progressive thermal demagnetization of the natural remanence with their associated statistics [K/α95] (Fisher, 1953) and their corresponding virtual geomagnetic north poles [VGPs]. Sites marked by * are the sites dominated by hematite with their means and paleomagnetic pole. ** Magnetite sites excluded from the means due to wide dispersion or intermediate directions.

Late Ypresion "Minia" Formation progressive thermal demagnetization results									
Site	N [demag.]	Soft [PDF] component			Anchored component				
		N	Dec./Inc. [°/°]	K/α95[°]	Mineral	N	Dec./Inc. [°/°]	K/α95[°]	North VGP [°N/°E]
Section I [28.0°N/30.85°E]									
I-1	7	3	15.5/54	23.4/26.1	Magnetite	7	168.4/−42.2	31.6/10.9	79/284.3
I-2	7	5	351/33.4	21.4/16.9	Magnetite	6	182.9/−22.7	34.8/11.5	73.6/200.8
I -3**	5	2	3.3/28.8	22.2/55.1	Magnetite**	3	179.1/−10.5	10.3/40.6	Wide α95
I -4	7	4	3.9/64.8	30.1/17	Magnetite	6	186.7/−3	30.8/12.3	62.7/196.1
I -5**	6	2	8/28	34.1/44.2	Magnetite**	6	86.4/66.7	10.9/21.2	Intermediate
I -6	7	1	351/42	-/-	Magnetite	7	15.8/23.3	37.4/10	68.3164.7
I -7	8	3	11.6/11.2	25.6/24.9	Magnetite	8	3.9/21	23.7/11.6	72.5/198
I -8*	8	6	353/21.3	30.7/12.3	Hematite*	8	3.3/46.7	13.5/15.7	87.1/121.2
I -9**	7	2	17.2/28.2	26.3/50.8	Magnetite**	4	355.9/41.3	14.4/25.1	Wide α95
I -10	7	3	341/72.3	27.1/24.2	Magnetite	6	185.8/−19.1	29.5/12.5	71.0/193.0
Mean of the magnetite anchored component of Section [I]						6sites/ 40 samples	184.5/−22	30.9/12.2	73.3/196.3 [A95=9.4°]
Section II [27.75°N/31.0°E]									
II-1*	6	5	7.2/21.3	20.2/17.4	Hematite*	6	345.1/51.5	15.9/17.3	76.4/323.5
II -2	8	4	334.7/29	39.6/14.8	Magnetite	7	182.1/−12.9	29.8/11.2	68.7/205.3
II 3	8	2	12/64	30.8/46.7	Magnetite	8	181.3/−43.1	34.1/9.6	87.1/187.2
II -4	6	4	346/14.2	18.3/22.1	Magnetite	5	198.1/−10.9	35.3/13.1	61.9/170
II -5**	5	4	26.6/33.3	25.3/18.6	Magnetite**	5	6.8/22.2	8.1/28.7	Wide α95
II -7	6	2	351.3/52	23/54.7	Magnetite	6	354/13.6	39.2/10.8	68.4/227.4
II- 8**	7	5	45/42	35.5/13	Magnetite**	5	64.9/62.8	9.7/25.9	Intermediate

Table 2 (*continued*)

Late Ypresion "Minia" Formation progressive thermal demagnetization results									
Site	N [demag.]	Soft [PDF] component			Anchored component				
		N	Dec./Inc. [°/°]	K/α95[°]	Mineral	N	Dec./Inc. [°/°]	K/α95[°]	North VGP [°N/°E]
II -9	8	1	341/27	-/-	Magnetite	8	193.8/−38.6	27.2/10.8	76.1/143.5
Mean of the magnetite anchored component of Section [II]						5 sites/ 34 samples	185.8/−24	20/17.5	74.6/189.2 [A95=12.9°]
Section III [27.5°N/30.5°E]									
III-1	8	6	10.5/48.5	23.4/14.1	Magnetite	8	178.3/−33.6	27.5/10.8	80.7/220.6
III-2*	7	4	355/62.2	31.3/16.7	Hematite*	5	5.3/37.4	19.9/17.6	81.8/173.1
III-4*	7	3	11/45	31.2/22.4	Hematite*	7	6.5/34.1	15.6/15.8	79.4/175.0
III-6	7	3	337.5/22	15/33	Magnetite	7	184.8/−1.4	26.2/12	62.8/200.0
III-7*	7	2	17/21	19.5/60	Hematite*	6	3.8/60.8	13.4/19	75.3/41.8
III-8	7	5	341/47	31.1/13.9	Magnetite	7	175.9/−22.8	24/12.6	73.9/225.1
Mean of the magnetite anchored component of Section [III]						3 sites/ 22 samples	179.9/−19.4	23/26.3	72.9/211.6 [A95=15.3]
Overall results of PCA best-fit lines of the progressive thermal demagnetization of the Late Ypresion "Minia" Formation [Three sections/ 24 sites/ 167 samples]									
24 sites	167 samples	Mean of PDF 24 sites/ 81 samp.	1.3/39.9	14.1/8.2	Mean of Magnetite	14 sites/ 96 samples	183.9/−22.2	28.1/7.6	73.8/197.5 [A95=5.6°]
					Mean of Hematite*	5 sites/32 samples	2/46.3	46.4/11.3	88.7/78.8 [A95=11.5°]

the hematite natural remanence is an extension of the PDF overprint in the studied samples and to the secondary depositional nature of the hematite remanence in these sites (Figs. 4, 5A lower part).

In each orthogonal projection, the differentiated components are visually isolated in each demagnetized sample. The direction of the best-fit line of at least three successive demagnetization steps of each component was calculated using the principal component analysis [PCA] technique (Kirschvink, 1980) and plotted for comparison (Fig. 5A).

6. Characteristic mean direction and paleomagnetic pole

The mean directions of the soft and the hard anchored components are calculated for each site with their associated statistical parameters; the precision parameter [K] and the semi-angle of the cone of 95% confidence [α95] (Fisher, 1953), in the three studied sections (Table 2, Fig. 5B).

The site-mean directions of the goethite-hosted soft component are, obviously, scattered around the present-day field direction in the study area (Fig. 5B upper part). The mean of this soft component, which is isolated in 24 sites/81 samples is at Dec./Inc. = 1.3°/39.9°, with K/α95 = 14.1/8.2°, (Table 2, Fig. 5C upper part), thus supporting their consideration as the present-day field overprint [Dec./Inc. = 2°/40°].

In fourteen sites (96 samples) spread in different stratigraphic levels in the studied sections, the site means of the anchored high-blocking temperature magnetite-hosted component, are characterized by bipolar antipodal N-S trending shallow inclination much shallower than the PDF (Table 2, Fig. 5B middle part). The section-mean of these magnetite-dominated sites is, separately, calculated for each section (Table 2). The overall mean of the Minia formation limestone magnetite anchored component is calculated for fourteen sites (96 samples) yielding a mean direction at Dec./Inc. = 183.9°/−22.8° with K/α95 = 28.1/7.6° (Table 2, Fig. 5C middle part). It is noteworthy to mention that the means of five of the magnetite sites have been, initially, rejected from further interpretation as they are widely dispersed or have intermediate directions (Table 2).

This anchored characteristic component of the magnetite passed the reversal test (McFadden and Lowes, 1981) at 95% confidence level. The reverse sites are eleven [Dec./Inc. = 183.8°/−22.8°] yielding a resultant at (R1 = 10.58) with a precision parameter (K1 = 23.87). The normal sites are three [Dec./Inc. = 4.4°/19.5°] yielding a resultant (R2 = 2.96) with a precision parameter K2 = 50.and the overall resultant was R = 13.54. Both normal and reverse components share a common mean at the 95% confidence level.

Based on its predominance in 3 sections/14 sites/96 samples with discernible deviation from the PDF direction and the positive reversal test at 95% confidence level, the magnetite-hosted anchored component was considered as the characteristic primary remanent direction of the Minia formation late Ypresion limestone. The virtual geomagnetic pole [VGP] of each site is calculated (Table 2) and plotted (Fig. 6A). The mean paleomagnetic north pole of the VGPs of the fourteen sites, which lies at 73.8°N/197.5°E (A95 = 5.6°) (Table 2, Fig. 6A), is considered as the paleomagnetic of Africa in the Late Ypresian (ca. 50 Ma).

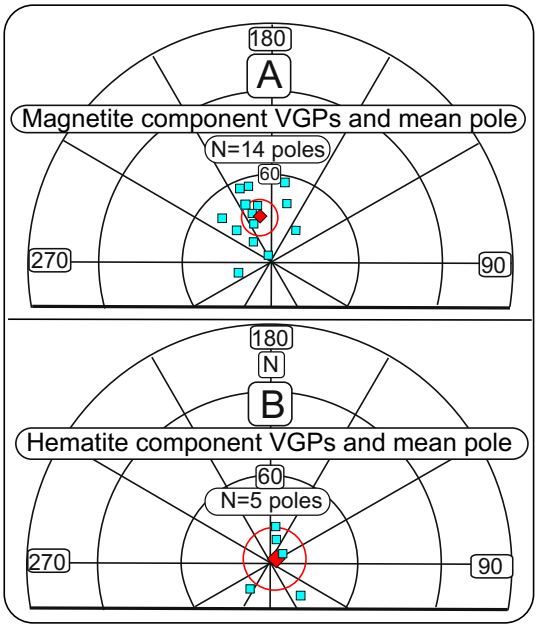

Fig. 6. Equal-area projections of the Virtual geomagnetic poles [VGPs] (squares) with their corresponding mean paleomagnetic north pole [diamonds] surrounded by its semi-angle cone of 95% confidence (A95) for the characteristic magnetite-hosted component [A] and the hematite component [B]. Data listed in Table 2.

Table 3
Original rotation parameters used for Euler Pole rotation with the interpolated parameters used in the present study calculated by the present authors.

Tectonic units rotated	Age	Chron.Anomaly	Rotation parameters [°]	Reference	Interpolated parameters	
					Age	Parameters[°]
Europe versus North America	49.71	An22o	64.52/138.18/−11.5	Gaina et al., 2002	50Ma	64.4/138.67/−11.605
	53.347	An240	63.07/144.26/−12.82			
Greenland versus North America	53.347	An24o	40.64/243.07/−3.615	in Torsvik et al., 2008	55Ma	27.5/229/3/−3.2
	55.9	An25y	20.5/221.8/−3			
North America versus Africa	46.3	An21	74.23/−5.01/15.106	Müller et al., 1997	50Ma	76.12/−2.95/16.23
	52.4	An24	77.34/−1.61/16.963			
	53.347	An24o	77.34/−1.61/16.963		55Ma	79.4/3.7/17.6
	55.9	An25y	80.54/6.57/17.895			
South America versus Africa	46.3	An21	56.95/−31.15/19.107	Müller et al., 1997	50Ma	58.15/−31.17/20.49
	52.4	An24	58.89/−31.18/21.38			

Table 4
Paleomagnetic north poles of the main tectonic units with their statistical parameters rotated to the African coordinates using the Euler pole rotation parameters in Table 3.
* Means calculated by the present authors.

North American Craton poles

Rock unit	Age [Ma]	K/A95 [°]	North Pole [°N/°E]	African Coord. [°N/°E]	Reference
East Fork Washakia Basin, WY	38–50 [44]	40/7.7	83.9/144 Co[76.7/230.4]	84.3/197.9 Co [73.2/252.4]	Flynn,1986
Absaroka flows, WY	45–50 [46]	15/8.4	83.5/177.4	82/221.6	Shive and Pruss, 1977
Rattlesnake Hill volcs, WY	42–50 [46]	14/9.6	79/146	79.9/182.2	Sheriff and Shive, 1980
Montery Intrs, VA, WV	42–49 [47]	21/10.1	85.2/244	81.4/266.5	Ressetar and Martin, 1980
Bitterroot Dome swarm, MT	47	−/5.6	72/161.6	72.1/189.4	Doughty and Sheriff, 1992
Robinson Anticline Intrs, MT	48–53 [50]	46/4	77.1/145.8	78.1/178.7	Harlan et al., 1988
Absaroka volcs, Wy	44–55]50]	17.6/7.8	82.5/137.1	83.6/183	Harlan and Morgan, 2010
Wasatch and Green River F., WY	51	−/4.9	77.6/129.1 Co[78.3/202.7]	79.7/161.3 [71/228]	Clyde et al., 1997
Comb. Eocene Intrs., MT	47–54 [51]	19/4	82/170	81/211.3	Diehl et al., 1983
Highwood Intrs, MT	51	15.4/7.1	81.2/167.3	80.5/207	Diehl et al., 1980
Bearpaw Intrs, MT	52	37/5.8	80.2/198.4	78/230.3	Diehl et al., 1980
Bighorn Basin, WY	55	−/4.4	81.4/167.7 Co[73.9/228.8]	80.7/207.8 Co[70.5/250.2]	Clyde et al., 2007
Mean N = 12 poles [uncorrected]*		216/2.9		81/201	
Mean N = 12 poles [corrected]*		113/4.1		79/220	

Stable Europe poles

Rock unit	Age	K/A95°	North pole	N. America	African coord.	Reference
Lower Paleogene London clay Fm.	52	−/6.8	63.7/178.6 Co[76.7/177.2	60.6/175.6 73.4/181.1	60/198.1 72.2/208.8	Ali et al., 2003
Lundy Island dikes, Scotland	49.5	−/1.5	82.6/155	80.3/174.8	79.2/211.3	Mussett et al., 1976
Sleat dikes, Skye,Scotland	51	/2	82/158	79.6/175.1	78.5/210.3	Wilson et al.,1982
Fishnish dikes, Scotland	52	15/10	74/139	73.7/145.8	74.8/174.8	Dagley and Mussett, 1978
Vaternish dike swarm, Scot.	55	21/3.5	76/160	73.9/166.5	73.6/195.6	Wilson et al., 1974
Faroe Islands Flood volcs,	55	24.5/4.5	71.4/154.7	69.9/157.8	70.3/184.2	Riisager, et al., 2002
Mean N = 6 poles*		237/4.4			75.2/196	

Greenland poles

Rock unit	Age	K/A95	North Pole	N. America	African Coord.	Reference
Scoresby Sund Lavas, E. Gd	55	369/4	69.7/181.4	71.7/185.3	71/212.1	Tarling et al., 1988
Kangerdlugsuaq dykes, E. Gd	54.5	57.5/6	63/180.4	65/182.2	64.5/207	Faller and Soper, 1979
Skaergaard Intrusion, E. Gd	55.5	40/4.2	61/165	63.4/165.8	63.8/189.7	Schwarz et al., 1979
Kangerdlugssuaq lavas, E. Gd	55.5	105/8.9	63.4/185.1	65.2/187.8	64.4/211.9	Faller, 1975
Jacobsen Fjord dykes, E. Gd	59	69/3.7	67.7/177.7	69.8/180.7	69.3/206.8	Faller and Soper, 1979
Fjord basalts, East Gd	56	240/9	64/184.5	66/187.2	65/211.5	Faller and Soper, 1979
Nuussuaq lavas, W. Gd	54	27.8/6.3	74.6/159.4	77.1/162	77.5/193.7	Riisager et al., 2003
Mean N = 7 poles*		159/4.8			68.2/204.5	

South America poles

Rock unit	Age	K/A95	North pole	African coord.	Reference
Eocene volcanics	47	–/5.7	81/157.4	74.1/214.6	Somoza, 2007
Patagonian Plateau basalt, Chile, Arg.	49	15/16.5	78/156.5	71.8/207.9	Butler et al., 1991
Andean intrusions, Chile	45	222/3.8	72.7/173	65.2/211	Dalziel et al., 1973
Mean N = 3 poles*		284/7.2		70.4/211	

Africa poles

Rock unit	Age	K/A95	North pole	Reference
Mokattam limestone, Egypt.	42.5	–/4.2	78.1/162.8	Abdeldayem, 1999
Fayum province limestone, Egypt*	44.5	–/6	70/159	Lotfy and Van der Voo, 2007
Wadi Abu Tereifiya basalt, Egypt	44.5	134/5.8	69.4/189.4	Hussain et al., 1979
Mean = 2 poles*			74/179.6	

On the other hand, five site means (38 samples) are found to be dominated by hematite remanence [blocking temperature Tb >600 °C]. These site-means are characterized by north-oriented positive medium inclination clustered around the present-day field in the study area (Table 2, Fig. 5B lower part). The overall mean direction of these sites, which is at Dec./Inc. = 2°/40.3°, is noticeably a parallel to the PDF direction (Table 2, Fig. 5C lower part). The virtual geomagnetic poles of these sites yield a high-latitude mean paleomagnetic north pole at 88.5°N/96°E [A95 = 10.8°] (Table 2, Fig. 6B). This component is considered as a present- day field overprint residing in epigenetic secondary hematite developed in the limestone upon their prolonged exposure to persistent desert weathering.

7. Discussion and comparison with global synchronous poles

The Minia formation late Ypresian paleomagnetic pole [73.8°N/197.5°E], was compared with coeval poles (ca. 50 Ma) rotated from the major tectonic plates to the African coordinates using the appropriate euler pole [EP] rotation parameters for each tectonic unit. The global poles were selected from some reliable databases (Van der Voo, 1993; McElhinny and Lock 1996; Pisarevsky, 2005) (Table 4). The present pole was compared with individual poles and mean poles of the North American Craton, Stable Europe, Greenland, South America and Africa (Tables 4 and 5, Fig. 7A). Further, it was compared with 50 Ma poles of some recent calculated apparent polar wander paths (Besse and

Table 5
The late Ypresian Paleomagnetic north poles of the African Plate with their semi-angle of the cone of 95% confidence around the mean pole [A95] and their corresponding paleo-directions and paleolatitudes at Cairo **[30°N/31°E]** as a reference location for comparison. NB. *Greenland poles are slightly older and are excluded from the overall mean of continents.

A. paleomagnetic north pole, paleo-directions and paleo-latitude of Cairo according to the present study

	Rock-unit	Age [Ma]	No of sites	A95[°]	North Pole [°N/°E]	Dec./Inc.	Paleo-Latitude
						Cairo reference [30°N/31°E]	
1	Late Ypresian "Minia formation"	50	14	5.6	73.8/197.5	3.9/26.8	14.2

B. Mean paleomagnetic north poles of the main tectonic units rotated to African coordinates

	Tectonic unit	Age [Ma]	No of poles	A95 [°]	North pole [°N/°E]	Dec./Inc.[°/°]	Paleo-latitude [°]
1a	N. American Craton corrected for inclination shallowing	50	12	4.1	79/220	358/34.7	19.1
1b	N. American Craton uncorrected for inclination	50	12	3	81/201	1.7/37.7	21.1
2	European Craton	50	6	4.4	75.2/196	3.9/29.3	15.7
3	Greenland	55*	7	4.8	68.2/204.5	2.4/16.3	8.3
4	South America	50	3	7.2	70.4/211	0/202	10.4
5	Africa	50	2		74/179.6	8.6/30	16.1
	Mean of 4 continents [corrected]	**50**	**4 cont,**	**6.5**	**75.1/200.9**	**2.7/28.7**	**15.3**
	Mean of 4 continents [uncorrected]	**50**	**4 cont.**	**5.1**	**75.5/197.3**	**3.5/29.6**	**15.9**

C. Mean north poles of some calculated apparent polar wander paths rotated to the African coordinates

	Calculated APWP	Age[Ma]	No of poles	A95[°]	North pole [°N/°E]	Dec./Inc.[°/°]	Paleo-latitude [°]
1	Torsvik et al., 2012	50	33	2.8	75.3/200.2	2.8/29.1	15.6
2	Torsvik et al., 2008	50	27	2.6	76.8/201.6	2.2/31.4	17
3	Courtillot, and Besse, 2004	50	38	2.9	75/211.3	0/28.2	15
4	Besse and Courtillot, 2002, 2003	50	31	3.4	76.9/210.3	0/31.3	16.9

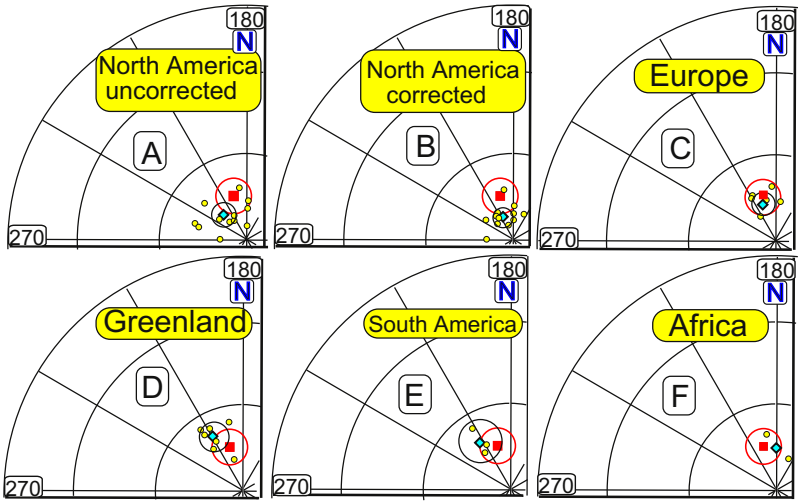

Fig. 7. A: Equal-area projections of the north paleomagnetic pole of the present study (square) with its semi angle cone of 95% confidence compared to the rotated poles (Circles) and mean paleomagnetic poles (diamonds) from the four main continents with their semi-angle cones of 95% confidence. B: Equal-area projections of the north paleomagnetic pole of the present study (square) with its semi angle cone of 95% confidence compared to the rotated mean poles of the four continents (circles), and the two overall means of the four continents (diamonds) and the synchronous poles of the calculated apparent polar wander path of Torsvik et al., (2008, 2012) (diamonds).

Courtillot, 2002, 2003; Courtillot and Besse, 2004; Torsvik et al., 2008, 2012), (Table 5, Fig. 7B).

Twelve poles representing the North America Craton between 44 and 55 Ma (Table 4A), were rotated to the African Plates using the rotation parameters of Müller et al. (1997). The rotation parameters were interpolated at 50 Ma using the original parameters of An 24 (52.4 Ma) and An 21 (46.3 Ma) (Table 3). Ten of the selected poles were driven from igneous rocks and two poles of sedimentary rocks. Two mean poles for the North American Craton were calculated and plotted (Tables 4A and 5, Fig. 7A) with and without correction for inclination shallowing errors, associated with their respective statistical parameters. Both North America mean poles have higher latitudes with respect to the present pole with partial overlap of their semi-angles of the cones of 95% confidence with the present pole (Table 5, Fig. 7A). However, the longitude of the American pole with the sedimentary poles uncorrected (201°E) fits well with the present pole (197.5°E), while the corrected mean pole shows some deviation.

Six poles representing Stable Europe between 45.5 and 55 Ma were selected. Only one pole was corrected for inclination shallowing. Europe poles were rotated to the North American Craton using the parameters cited in Table 1 (Torsvik et al., 2008) at 50 Ma between An 24o [53.347 Ma] and An 22o [49.71 Ma] (Table 3). These are, then, rotated from North America to Africa using the parameters of Müller et al., (1997) interpolated between An 24 [52.4 Ma] and An 21 [46.3 Ma] (Table 3). The mean Europe rotated poles [50 Ma] (Table 4B) fits quite well with the Minia formation pole. The semi angle of the cone of 95% confidence of the present pole lies inside the cone of the mean Europe pole and the European poles are clustered around both poles (Table 5, Fig. 7A).

In the global databases, the poles of Greenland are slightly older than the present pole. Seven poles driven from Tertiary igneous rocks of Greenland ranging between 54 and 59 Ma were selected. These poles were rotated to the North American Craton using the parameters cited in Table 1 (Torsvik et al., 2008), then rotated to Africa using the parameters of Müller et al., 1997 (Table 3). The rotation parameters were interpolated at 55 Ma between An 25y (55.9 Ma) and An 24o (53.347 Ma) (Table 3). The mean of the rotated Greenland pole was calculated with its associated statistical parameters (Tables 4C and 5) and plotted (Fig. 7A). Taking into consideration that Greenland poles which are mainly Paleocene age (54–59 Ma) are older than the present pole (50 Ma), the Greenland pole has a slightly lower latitude 68.2°N than the present pole (73.5°N) with partially overlapping semi angles of their cones of 95% confidence (Table 5, Fig. 7A).

Only three South American poles ranging between 45 and 49 Ma were selected. These poles which are slightly younger than the present pole originate from igneous rocks. These South American were rotated to Africa using the rotation parameters of Müller et al., (1997), interpolated at 50 Ma between the original rotation parameters of An 24 [52.4 Ma] and An 21 [46.3 Ma] (Tables 3 and 4D). The South America mean pole with its semi angle cone of 95% confidence largely overlaps with the Minia formation pole with slightly lower latitude (Table 5, Fig. 7A).

The three Egyptian poles which were found to represent the African Plate between 42.5 and 44.5 Ma, are slightly younger than the present pole. Two of these poles are driven from Eocene limestone and the third from Tertiary basalts. However, the Fayoum province limestone pole (Lotfy and Van der Voo, 2007), was excluded from the African mean pole due the declination deviation referred to possible local structural rotation in Fayoum province (Lotfy and Van der Voo, 2007). The mean of the two remaining African poles lies along the same latitude of the present pole with slightly deviating longitude (Tables 4 and 5, Fig. 7A).

Two overall mean poles for the mean rotated poles of the four continents; North America, Europe, South America and Africa, were calculated with two different North American Craton poles corrected and uncorrected for inclination shallowing error (Table 5, Fig. 7B). Greenland mean was excluded from these overall means as they are driven from Paleocene igneous rocks [54–58 Ma]. Both means of the four continents fit perfectly with the present pole, with complete overlap of their semi angle of the cones of 95% confidence and the four continents poles are clustered around the Minia formation pole (Table 5, Fig. 7B).

The Lower Eocene pole of the present study was, also, compared with some recent calculated apparent polar wander paths; Besse and Courtillot, 2002, 2003; Courtillot and Besse, 2004; Torsvik et al., 2008, 2012, (Table 5, Fig. 7B). Despite that the latitudes of the calculated poles [50 Ma] of Besse and Courtillot (2002), Besse and Courtillot (2003); Courtillot and Besse(2004), which lie at 76.9°N and 75°N are close the present latitude 73.5°N (Table 5), yet their longitudes (210.3°E, 211.3°E) are deviating. This deviation could be referred to the poles selected and the rotation parameters applied to calculate these APWPs. On the other hand, the present pole [73.8°N/197.5°E] fits quite well with the 50 Ma poles of Torsvik et al., 2008, 2012, [76.8°N/201.6°E and 75.3°N/200.2°E, respectively (Table 5, Fig. 7B).

8. Conclusions

The present paleomagnetic study on the isotropic late early Eocene Minia formation limestone, successfully, isolated a stable bipolar shallow characteristic remanent magnetic [ChRM] component residing in magnetite all over the stratigraphic intervals of the three studied sections. The paleomagnetic north pole of this characteristic remanence [73. 8°N/197.5°E], which is in reasonable consistency with synchronous global poles from the main tectonic units, can be considered as representing the African Plate in the late Ypresian time. This pole places the African Plate at far south latitudes with respect to its present day latitudinal position. The location of Cairo, which lies now at 30°N in northeast Africa, was at a paleolatitude of 14°N in the late early Eocene, i.e. 16° of latitude south of its present latitude (Fig. 8).

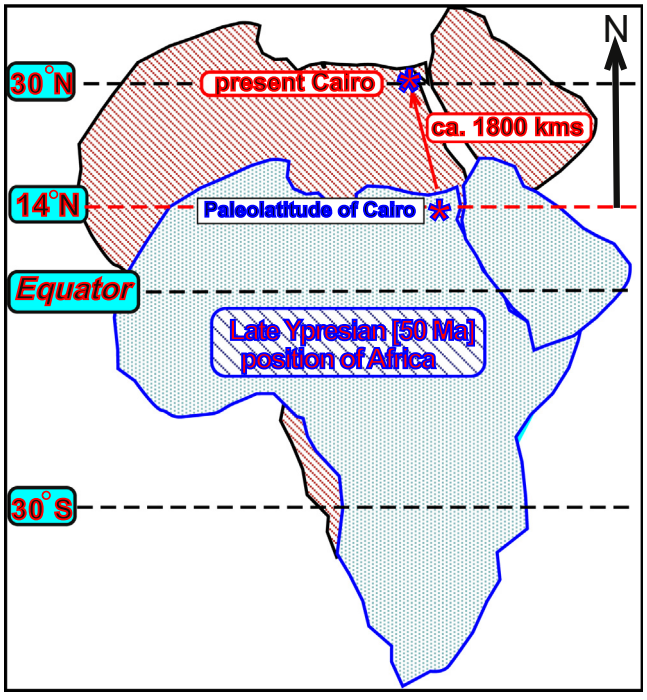

Fig. 8. The Late Ypresian paleotectonic position of the African continent compared to the present-day position of Africa.

References

Abdeldayem, A.L., 1999. Palaeomagnetism of some Cenozoic sediments, Cairo-Fayum area. Egypt. Phys. Earth Planet. Intr. 110, 71–82.

Ali, J.R., Ward, D.J., King, C., Abrajevitch, A., Liu, Z., Zhao, X., Wang, C., Liu, S.Y.H., 2003. First Palaeogene sedimentary rock palaeomagnetic pole from stable western Eurasia and tectonic implications. Geophys. J. Int. 154, 463–470.

Balsley, J.R., Buddington, A.F., 1960. Magnetic susceptibility anisotropy and fabric of some Adirondack granites and orthogneisses. Am. J. Sci., 258 A, 6–20.

Bayoumi, A.I., Lotfy, H.I., 1987. Modes of structural evolution of Abu Gharadig basin, Western Desert of Egyot, as deduced from seismic data. J. Afr. Earth Sci. 9, 273–287.

Besse, J., Courtillot, V., 2002. Apparent and true polar wander and the geometry of the geomagnetic field over the last 200 Myr. J. Geophys. Res. 107, B11, 1978–2012, 2300, https://doi.org/10.1029/2000JB000050.2002.

Besse, J., Courtillot, V., 2003. Correction to apparent and true polar wander and the geometry of the geomagnetic field over the last 200 Myr. J. Geophys. Res. 108 (B10), 2469. https://doi.org/10.1029/2003JB002684.

Bishay, Y., 1961. Biostratigraphic study of the Eocene in the Eastern Desert between Samalut and Assiut by the larger Foraminifera. Third Arab Petrol. Congr, Alexandria, Egypt, p. 7p.

Boukhary, M., Abdelmalik, W., 1983. Revision of the stratigraphy of the Eocene deposits of Egypt. N. Jb. Geol. Palaeont. Mh. 6, 321–337.

Boukhary, M., Blondeau, A., Ambroise, D., 1982b. Etude sur les nummulites de la region de Minia- Samalut, Vallee du Nil, Egytp, 2. Multivariate analysis. 8th Afr. Micropaleontol. Colloq., Paris. Cah. Micropaleontol. 1, 78–89.

Boukhary, M., Blondeau, A., Ambroise, D., 1982a. Etude sur les nummulites de la region de Minia- Samalut, Vallee du Nil, Egytp, 1. Biometrie et biostratigraphie. 8th Afr. Micropaleontol. Colloq., Paris Cah. Micropaleontol. 1, 65–78.

Butler, R.F., Herve, F., Munizaga, F., Beck Jr., M.E., Burmester, R.F., Oviedo, E.S., 1991. Paleomagnetism of the Patagonian Plateau Basalts, southern Chile and Argentina. J. Geophys. Res. 96 (B4), 6023–6034.

Cande, S.C., LaBreceque, J.L., Haxby, W.F., 1988. Plate kinematics of the South Atlantic: Chron C34 to present. J. G. R. 93, 13479–13492.

Clyde, W.C., Hamzi, W., Finarelli, J.A., Wing, S.L., Schankler, D., Chew, A., 2007. Basin-wide magnetostrtigraphic framework for the Bighorn Basin, Wyoming, GSA Bull., 109, 7/8, 848–859.

Clyde, W.C., Zenneveld, J.-P., Stamatakos, J., Gunnell, G.F., Bartels, W.S., 1997. Magnetostratigraphy across the Wasatchian- Bridgerian boundary (early to middle Eocene) in the western Green River Basin. Wyoming. J. Geol. 105, 657–669.

Courtillot, V., Besse, J., 2004. A long-term Octupolar Component in the Geomagnetic Field? (0-200 Million Years B. P.). In: Channell, J.E.T., Kent, D.V., Lowrie, W, Meert J.G., (Eds.), Timescales of the Paleomagnetic Field, Geophysical Monograph Series, 145, Am. Geophys. Union, Washington D.C., 59–74. (10-1029/145GMOS).

Dagley, P., Mussett, A.E., 1978. Palaeomagnetism of the Fishnish dykes, Mull. Scotland. Geophys. J. R. Astr. Soc. 53 (3), 553–558.

Dalziel, I.W.D., Lowrie, W., Kligfield, R., Opdyke, N.D., 1973. Paleomagnetic data from the southernmost Andes and the Antarctandes. In: Tarling, D.H., Runcorn, K.S. (Eds.), Implication of Continental drift of Earth Sciences. Academic Press, San Diego California, pp. 87–101.

Dewey, J.F., Helman, M.L., Turco, E., Hutton, D.H. W., Knott, S.D., 1989. Kinematics of the western Mediterranean, In: Coward, M.P., Dietrich, D., Park, R.G., (Eds.), Alpine tectonics: Geol. Soc, London Special Publ., 45, 265– 283.

Diehl, J.F., Beske-Diehl, S., Beck Jr., M.E., Hearn Jr., B.C., 1980. Paleomagnetic results from Early Eocene Intrusion, north-central Montana: Implications for North American polar-wandering. Geophys. Res. Lett. 7 (7), 541–544.

Diehl, J.F., Beck Jr., M.E., Beske-Diehl, S., Jacobson, D., Hearn Jr., B.C., 1983. Paleomagnetism of the Late Cretaceous- early Tertiary morth- central Montana alkalic province. J. Geophys. Res., 88, 10,593–10,609.

Doughty, T.P., Sheriff, S.D., 1992. Paleomagnetic evidence for en echelon crustal extension and crustal rotations in western Montana and Idaho. Tectonics 11 (3), 663–671.

Ellwood, B.B., Crick, R.E., 1988. Paleomagnetism of Paleozoic asphaltic deposits in southern Oklahoma USA. Geophys. Res. Lett. 15, 436–439.

Faller, A.M., 1975. Palaeomagnetism of the oldest Tertiary Basalts in the Kangerdlugssuaq area of East Greenland. Geol. Surv. Den. Geen. Bull. 24, 173–178.

Faller, A.M., Soper, N.J., 1979. Palaeomagnetic evidence for the origin of the coastal flexure and dyke swarm in central East Greenland. J. Geol. Soc. London 136, 737–744.

Fisher, R.A., 1953. Dispersion on a sphere. Proc. R. soc. London Ser. A 217, 295–305.

Flynn, J.J., 1986. Correlation and geochronology of the middle Eocene strata from western United States. Palaeogeogr. Palaeoclimatol. Palaeoecol. 55, 335–406.

Gaina, C., Roest, W.R., Muller, R.D., 2002. Late Cretaceous-Cenozoic deformation of northeast Asia. Earth Planet. Sci. Lett. 197, 273–286. https://doi.org/10.1016/50012-821X(02)00499-5.

Granar, L., 1958. Magnetic measurements on Swedish varved sediments. Ark. Geofys. 3, l–40.

Guiraud, R., Issawi, B., Bellion, Y., 1985. Les lineaments guineo- nubiens un trait structural majeur a l'echelle de la plaque africaine. C. R. Acad. Sc. Paris 300, 17–20.

Gumati, Y.D., Kanes, W.H., 1985. Early Tertiary subsidence and sedimentary facies; northern Sirte basin. Libya. AAPG Bull. 69, 39–52.

Haq, B.U., Hardenbol, J., Vail, P.R., 1988. Mesozoic and Cenozoic Chronostratigraphy and cycles of sea- level changes. In: Sea- Level Changes: An Integrated Approach. Soc. Geo. Paleont. Min. Special Publ. 42, 71–108.

Harlan, S.S., Morgan, L.A., 2010. Paleomagnetic results from Tertiary volcanic strata and intrusions, Absaroka volcanic supergroup, Yellowstone National Park and vicinity. Contributions of the North American apparent polar wander path. Tectonophysics 485 (1), 245–259.

Harlan, S.S., Geissman, J.W., Lageson, D.R., Snee, L.W., 1988. Isotopic dating of thrust- belt deformation along the eastern edge of the Helena salient, northern Crazy Mountains Basin. Montana. Geol. Soc. Am. Bull. 100, 492–509.

Heller, F., 1978. Rock magnetic studies of Upper Jurassic limestones from southern Germany. J. Geophys. 44, 525–543.

Hussain, A.G., Schult, A., Soffel, H., 1979. Palaeomagnetism of the basalts of wadi Abu Tereifiya, Mandisha, and dioritic dykes of wadi Abu Shihate. Egypt. Geophys. J. Int. 56 (1), 55–61.

Issawi, B., El Hinnawi, M., Francis, M., Mazhar, A., 1999. The Phanerozoic Geology of Egypt, a Dynamic Approach. Egyptian Geol. Surv, Cairo, p. 462p.

Jelinek, V., 1981. Characterization of the magnetic fabric of rocks. Tectonophysics 79, 63–67.

Jelinek, V., 1978. Statistical processing of anisotropy of magnetic susceptibility measured on groups of specimens; Studia Geophysica et Geodetica. 22, 50–62.

Kirschvink, J.L., 1980. The least squares line and plane and the analysis of paleomagnetic data. Geophys. J. R. Astr. Soc. 62, 699–718.

Klitzsch, E., List, F., Föhlmann, G., 1987. Geological map of Egypt, 1:500 000, Asyut sheet [NG 36 NW] and Beni Suef sheet [NH 36 SW]. The Egyptian Petroleum Corporation- Conoco Coral, Cairo, Egypt.

Lotfy, H.I., der Voo, Van, 2007. Tropical northeast Africa in the middle-late Eocene: Paleomagnetism of the marine mammals sites and basalts in thr Fayum province. J. Afr. Earth Sci. 47, 135–152.

Lowrie, W., 1990. Identification of ferromagnetic minerals in a rock by coercivity and unblocking temperature properties. Geophys. Res. Lett. 17 (2), 159–162.

McElhinny, M.W., Lock, J., 1996. IAGA paleomagnetic databases with access. Surv. Geophys. 17 (5), 575–591. 19.1038/2161276a0.

McFadden, P.L., Lowes, F.J., 1981. The discrimination of mean directions drawn from Fisher distributions. Geophys. J. R. Astr. Soc. 67, 19–33.

Müller, R.D., Roest, W.R., Royer, J.Y., Gahagan, L.M., Sclater, J.G., 1997. Digital isochrones of the world's ocean floor. J. Geopgys. Res. 102, 3211–3214.

Mussett, A.E., Dagley, P., Eckford, M., 1976. The British Tertiary igneous province: Palaeomagnetism and age of dykes, Lundy Island. Bristol Channel. Geophys. J. Int. 46 (3), 595–603.

Nagata, T., 1961. Rock Magnetism. Maruzen, Tokyo, p. 350p.

Nürnberg, D., Müller, R., 1991. The tectonic evolution of the South Atlantic from Late Jurassic to present. Tectonophysics 191, 27–53.

Patriat, P., Achache, J., 1984. India- Eurasia collision chronology has implications for crustal shortening and driving mechanism of plates. Nature 311, 615–621.

Patriat, P., Segoufin, J., 1988. Reconstruction of the Central Indian Ocean Tectonophysics, 155, 211–234.

Philobbos, E.R., Keheila, E.A., 1979. Depositional environments of the middle Eocene in the area southeast of Minia. Egypt. Ann Geol. Surv. Egypt 9, 523–550.

Pisarevsky, S.A., 2005. New edition of the global Paleomagnetic database. EOS 86 (17), 170.

Ressetar, R., Martin, D.L., 1980. Paleomagnetism of Eocene igneous intrussives in the Valley and Ridge Province, Virginia and West Virginia. Can. J. Earth Sci. 17, 1583–1587.

Riisager, P., Riisager, J., Abrahamsen, N., Wagastein, R., 2002. New paleomagnetic pole and magnetostratigraphy of Faroe Islands flood volcanics, North Atlantic igneous province, Earth Planet. Sci. Lett. 201, 261–276.

Riisager, P., Riisager, J., Pedersen, A.K., 2003. Paleomagnetism of large igneous provinces: case-study from West Greenland, North Atlantic igneous province. Earth Planet. Sci. Lett. 214, 406–425.

Rochette, P., Jackson, M., Aubourg, C., 1992. Rock magnetism and the interpretation of anisotropy of magnetic susceptibility. Rev. Geophys. 30, 209–226.

Said, R., 1990. Cenozoic. In: Said, R. (Ed.), The Geology of Egypt. Balkema, Rotterdam, A. A, pp. 451–486.

Said, R., 1960. Planktonic foraminifera from the Thebes Formation, Luxor. Micropalaeontology, 6, 277–296.

Said, R., 1962. The Geology of Egypt, Elsevier., pp. 377.

Schwan, W., 1980. Geodynamic peaks in Alpinotype orogenies and changes in ocean-floor spreading during Late Jurassic- late Tertiary time. AAPG Bull. 64, 359–373.

Schwarz, E.J., Coleman, L.C., Cattroll, H.M., 1979. Paleomagnetic results from the Skeargaard intrusion, East Greenland, Earth Planet. Sci. Lett. 42, 437–443.

Sheriff, S.D., Shive, P.N., 1980. The Rattlesnake Hills of central Wyoming revisited: further paleomagnetic results. Geophys. Res. Lett. 7, 589–592.

Shive, P.N., Pruss, E.F., 1977. A paleomagnetic study of Basalt flows from the Absaroka Mountains. Wyoming. J. Geophys. Res. 82, 3039–3048.

Somoza, R., 2007. Eocene paleomagnetic pole from South America: Northward continental motion in the Cenozoic, opening of Drake Passage and Caribean convergence. J. Geophys. Res. 112, B03104. https://doi.org/10.1029/2006JB004610.

Stacey, F.D., Joplin, G., Lindsay, J., 1960. Magnetic anisotropy and fabric of some foliated rocks from S. E. Australia. Geophysica pure Appl. 47, 30–40.

Tarling, D.H., Hailwood, E.A., Lovlie, R., 1988. A palaeomagnetic study of lower Tertiary lavas in E. Greenland and comparison with other lower Tertiary observations in the northern Atlantic. In: Morton, A.C., Parson, L.M. (Eds.), Early

Tertiary Volcanism and the opening of the NE Atlantic. Geological Society Special Publication, vol. 39, pp. 215–224.
Tarling, D.H., Hrouda, F., 1993. The Magnetic Anisotropy of Rocks. Chapman and Hall, London, p. 213.
Torsvik, T.H., Muller, R.D., Van der Voo., R., Steinberger, B., Gaina, C., 2008. Global plate motion frames: Towards a unified model. Rev. Geophys. 46, RG3004., https://doi.org/10.1029/2007/RG000227.
Torsvik, T.H., Van, R., der Voo, Preeden, U., MacNiocaill, C., Steinberger, B., Doubrovine, P.V., van Hinsbergen, D.J.J., Domeier, M., Gaina, C., Tohver, E., Meert, J., McCausland, P.J.A., Cocks, L.R.N., 2012. Phanerozoic polar wander: paleogeography and dynamics. Earth Sci. Rev. 114, 325–368.
Van der Voo, R., 1993. Paleomagnetism of the Atlantic. Cambridge University Press, Tethys and Iapetus Oceans, p. 411.
Wilson, R.L., Ade-Hall, J.M., Skelhorn, R.R., Speight, J.M., Dagley, P., 1974. The British Tertiary Igneous Province: Palaeomagnetism of the Vaternish dyke swarm on North Skye, Scotland. Geophys. J. R. Astr. Soc., 37 (1), 23–30.
Wilson, R.L., Hall, J.M., Dagley, P., 1982. The British Tertiary Igneous Province: Palaeomagnetism of the dyke swarm along Sleat coast of Skye. Geophys. J. R. Astr. Soc. 68, 317–323.
Zijderveld, J.D.A., 1967. A. C. demagnetization of rocks. In: Collinson, D.W, Creer, K. M. Runcorn. S.K., (Eds.) Methods in Paleomagnetism, Elsevier, New York. pp. 256–286.